

# DreamGaussian4D: Generative 4D Gaussian Splatting

Jiawei Ren<sup>\*1</sup> Liang Pan<sup>\*2</sup> Jiaxiang Tang<sup>13</sup> Chi Zhang<sup>1</sup> Ang Cao<sup>4</sup> Gang Zeng<sup>3</sup> Ziwei Liu<sup>1</sup>

<https://jiawei-ren.github.io/projects/dreamgaussian4d>

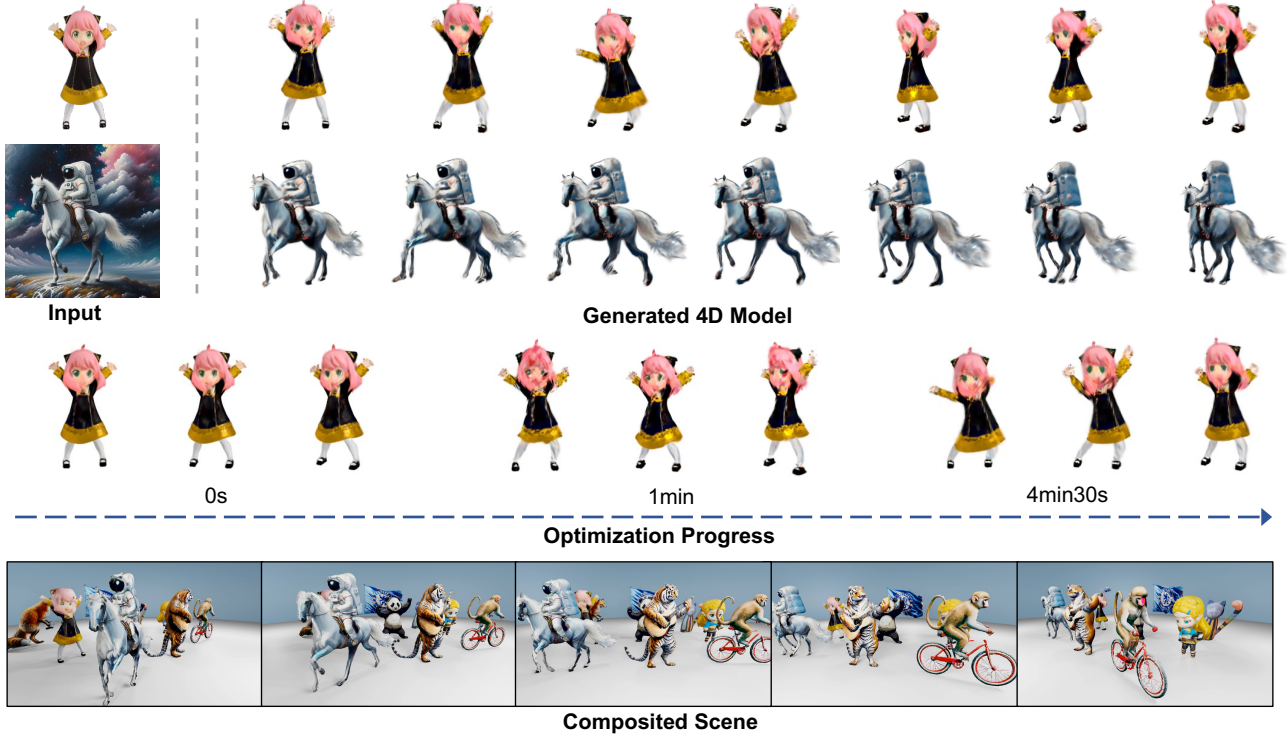


Figure 1: **DreamGaussian4D** generates 4D contents in minutes by leveraging 4D Gaussian Splatting. Exported meshes can be efficiently composited and rendered in 3D engines.

## Abstract

Remarkable progress has been made in 4D content generation recently. However, existing methods suffer from long optimization time, lack of motion controllability, and a low level of detail. In this paper, we introduce DreamGaussian4D, an efficient 4D generation framework that builds on 4D Gaussian Splatting representation. Our key insight is that the explicit modeling of spatial transformations in Gaussian Splatting makes it more suitable for the 4D generation setting compared with implicit representations. DreamGaussian4D reduces the optimization time from several hours

Table 1: **Speed Comparison.** DreamGaussian4D reduces the optimization time from several hours to several minutes.

Method	Time	Iterations
MAV3D (Singer et al., 2023)	6.5 hr	12k
Animate124 (Zhao et al., 2023)	-	20k
Consistent4D (Jiang et al., 2023)	2.5 hr	10k
4D-fy (Bahmani et al., 2023)	23 hr	120k
Dream-in-4D (Zheng et al., 2023)	10.5 hr	20k
AYG (Ling et al., 2023)	-	20k
DreamGaussian4D (Ours)	<b>6.5 min</b>	<b>0.7k</b>

to just a few minutes, allows flexible control of the generated 3D motion, and produces animated meshes that can be efficiently rendered in 3D engines. Code is available at [github.com/jiawei-ren/dreamgaussian4d](https://github.com/jiawei-ren/dreamgaussian4d).

<sup>1</sup>S-Lab, Nanyang Technological University <sup>2</sup>Shanghai AI Laboratory <sup>3</sup>Peking University <sup>4</sup>University of Michigan. Correspondence to: Ziwei Liu <ziwei.liu@ntu.edu.sg>.

## 1. Introduction

Remarkable progress has been witnessed in generative models, demonstrating significant recent advancements and innovations in generating diverse digital content, such as 2D images (Rombach et al., 2022; Sheynin et al., 2022), videos (Wang et al., 2023; Blattmann et al., 2023), and 3D scenes (Jun & Nichol, 2023; Hong et al., 2023; Tang et al., 2023a). While a few recent research works (Singer et al., 2023; Jiang et al., 2023; Zhao et al., 2023; Bahmani et al., 2023) have been devoted to 4D generation, achieving consistency and high quality in the generation of dynamic 4D scenes is far from being fully resolved.

4D dynamic scenes are often represented by using 4D dynamic Neural Radiance Fields (NeRF), which are expected to show consistent appearance, geometry, and motions from arbitrary viewpoints. By combining the benefits of video and 3D generative models, MAV3D (Singer et al., 2023) achieves text-to-4D generation by distilling text-to-video diffusion models on a Hexplane (Cao & Johnson, 2023). Consistent4D (Jiang et al., 2023) introduces a video-to-4D framework to optimize a Cascaded DyNeRF for 4D generation from a statically captured monocular video. With multiple diffusion priors, Animate124 (Zhao et al., 2023) could animate a single in-the-wild image into 3D videos through textural motion descriptions. Using a hybrid SDS, 4D-fy (Bahmani et al., 2023) achieves compelling text-to-4D generation based on multiple pre-trained diffusion models. However, they (Singer et al., 2023; Jiang et al., 2023; Zhao et al., 2023; Bahmani et al., 2023) tend to take hours to generate a 4D NeRF, and also their generated motions could not be well-controllable.

In this work, we introduce the DreamGaussian4D framework, which could efficiently generate dynamic scenes with 4D Gaussian splatting (4D GS) in just a few minutes. Our key insight is that the explicit modeling of spatial transformation in Gaussian Splatting significantly simplifies the dynamic optimization in 4D generation. We first fit a static 3D Gaussian Splatting (3D GS) using the image-to-3D frameworks introduced in DreamGaussian (Tang et al., 2023a). We propose a better training recipe, DreamGaussianHD, that alleviates the under-optimization problem in DreamGaussian. For the dynamic optimization, we learn the motion from a driving video in replace of the commonly used score distillation from video diffusion models. The driving video is generated from image-to-video diffusion models and enables better controllability and motion diversity. Finally, we export the 4D GS to an animated mesh sequence and refine the per-frame texture map with a video-to-video pipeline that improves temporal coherence.

In summary, our contributions are as follows:

1. We employ the deformable Gaussian Splatting repre-

sentation in 4D content generation, and observe that its explicit spatial transformation modeling significantly reduces the optimization time from several hours to just a few minutes.

2. We design an image-to-4D framework that learns motion from image-conditioned generated videos, allowing more controllable and diverse 3D motions.
3. We propose a video-to-video texture refinement strategy that further enhances the quality of exported animated meshes, making the framework easier to deploy in a real-world setting.

## 2. Related works

### 2.1. 4D Representations

Thrilling progress has been observed in representing dynamic 3D scenes (4D scenes). One line of research directly represents 4D scenes as a function of  $x, y, z$  with additional time dimension  $t$  or latent code (Xian et al., 2021; Gao et al., 2021; Li et al., 2022; 2021). Another line of work represents 4D scenes as the combination of deformation fields with static canonical 3D scenes (Pumarola et al., 2021; Park et al., 2021a;b; Du et al., 2021; Tretschk et al., 2021; Yuan et al., 2021; Li et al., 2023). A crucial bottleneck of 4D representation is its speed, which takes dozens of hours for a single scene. Numerous approaches are explored to solve this problem. Notably, using explicit or hybrid representations archives impressive results, including planar decomposition for 4D space-time grid (Cao & Johnson, 2023; Fridovich-Keil et al., 2023; Shao et al., 2023), hash representation (Turki et al., 2023), and other structures (Fang et al., 2022; Abou-Chakra et al., 2024; Guan et al., 2022). Very recently, Gaussian Splatting (Kerbl et al., 2023) has drawn significant attention as it provides both satisfactory speed and impressive reconstruction quality. Extending static Gaussian Splatting into dynamic versions becomes a promising direction. Dynamic 3D Gaussians (Luiten et al., 2023) optimize per-frame Gaussian Splatting with dynamic regularizations and shared size, color, and opacity. 4D Gaussian Splatting (Wu et al., 2023; Yang et al., 2023) uses a deformation network to predict time-dependent position, scale, and rotation deformation.

### 2.2. Image-to-3D Generation

Image-to-3D generation aims at generating 3D assets from a single reference image. It can be viewed as a conditional generation task using techniques like diffusion models (Ho et al., 2020). Point-E (Nichol et al., 2022) and Shap-E (Jun & Nichol, 2023) can be directly trained to generate 3D point clouds or Neural Radiance Fields (NeRF) (Mildenhall et al., 2020) conditioned on image features, but the quality is restricted by spatial resolution and high-quality

3D datasets. Some methods (Melas-Kyriazi et al., 2023; Tang et al., 2023b) take advantage of recent performant 2D diffusion models (Rombach et al., 2022; Liu et al., 2023c; Deitke et al., 2023a) and lift them to 3D using score distillation sampling (SDS) (Poole et al., 2022). For example, Magic123 (Qian et al., 2023) combines both image and text input to distill high-quality 3D models through NeRF. DreamGaussian (Tang et al., 2023a) further shortens the optimization time using the Gaussian splatting representation (Kerbl et al., 2023). The problem can also be formulated as a single-view 3D reconstruction task. Many works (Xu et al., 2019; Chen & Zhang, 2019; Chen et al., 2020; Trevithick & Yang, 2021; Duggal & Pathak, 2022; Szymanowicz et al., 2023) adopt auto-encoder structures to learn 3D priors for this ill-posed task but are typically limited to one or a few categories of synthetic objects (Chang et al., 2015). Recently, One-2-3-45 (Liu et al., 2023b;a) uses 2D diffusion models (Liu et al., 2023c; Shi et al., 2023) to generate multi-view images and train an efficient multi-view reconstruction model. LRM (Hong et al., 2023) adopts transformer-based architecture to scale up the task on large datasets (Deitke et al., 2023b; Yu et al., 2023) by directly regressing a triplane-based NeRF.

### 2.3. 4D Generation

4D generation aims to generate dynamic 3D scenes, which are useful in a wide range of graphics applications including animation, gaming, and virtual reality. One line of work is to leverage text-to-video diffusion models to distill 4D contents (Singer et al., 2023). Concretely, they optimize a 4D representation like Hexplane (Cao & Johnson, 2023) or K-plane (Fridovich-Keil et al., 2023) by synthesizing camera trajectories and then computing SDS on rendered videos. Recent works focus on further improving photorealism by introducing combining multiple diffusion priors in pursuit of a stronger supervision signal (Bahmani et al., 2023; Zheng et al., 2023). However, the optimization time and computation cost are prohibitive for these approaches to be deployed in the real world. Moreover, the 3D contents couple with motions, therefore they lack diversity and control of the generated motions. Recently, a few works have proposed to obtain the 4D model from an input image (Zhao et al., 2023). However, they still adhere to the video distillation framework and suffer from prolonged optimization times and a lack of effective motion control. Notably, Consistent4D (Jiang et al., 2023) proposes to obtain the 4D model from an input video, which is closest to our setting. Compared to it, we study image-conditioned generated videos, which allow diverse motions on the same static model. A concurrent work (Ling et al., 2023) also explores Gaussian Splatting for high-quality 4D generation and our approach requires less than 5% of its optimization iterations in comparison.

## 3. Approach

DreamGaussian4D comprises three stages. The initial stage, static generation, involves designing an enhanced variant of DreamGaussian (Tang et al., 2023a) to create 3D Gaussians from the input image (Section 3.1). The second stage, dynamic generation, generates a driving video from the input image to optimize a time-dependent deformation field upon the static 3D Gaussians (Section 3.2). The final stage is an optional mesh refinement that converts the 4D Gaussians into an animated mesh sequence and applies a video-to-video pipeline to refine the texture maps consistently (Section 3.3).

### 3.1. DreamGaussianHD for Static Generation

Despite its rapid optimization speed, the original DreamGaussian (Tang et al., 2023a) introduces significant blurriness to the unseen areas of static models, as illustrated in Figure 7. This blurriness adversely affects the subsequent dynamic optimization process. Therefore, we first design better implementation practices to reliably enhance the image-to-3D generation quality of DreamGaussian at the cost of a reasonable increase in optimization time. We summarize these improved practices as DreamGaussianHD.

#### 3.1.1. MULTI-VIEW OPTIMIZATION

Apart from the reference view, DreamGaussian typically samples one random view at each optimization iteration for SDS. This approach covers only part of the Gaussians and leads to unbalanced optimization and convergence. As observed in previous works, increasing the number of sampled views (batch size) at each optimization step can significantly mitigate this issue (Poole et al., 2022; Chen et al., 2023). Sampling 16 views, for instance, yields high-quality geometry in the unseen regions of the 3D Gaussians. As a trade-off, this approach incurs an increase in memory usage during SDS computation and lengthens the optimization duration.

#### 3.1.2. FIXING BACKGROUND COLOR

DreamGaussian uniformly samples the background color from black and white. However, most 3D-aware image diffusion models render the training objects with a white background. We have observed that renderings with a black background introduce additional noise into the optimization process, ultimately resulting in blurriness. By consistently setting the background color to white, we achieve more detailed and refined results in the optimized 3D GS.

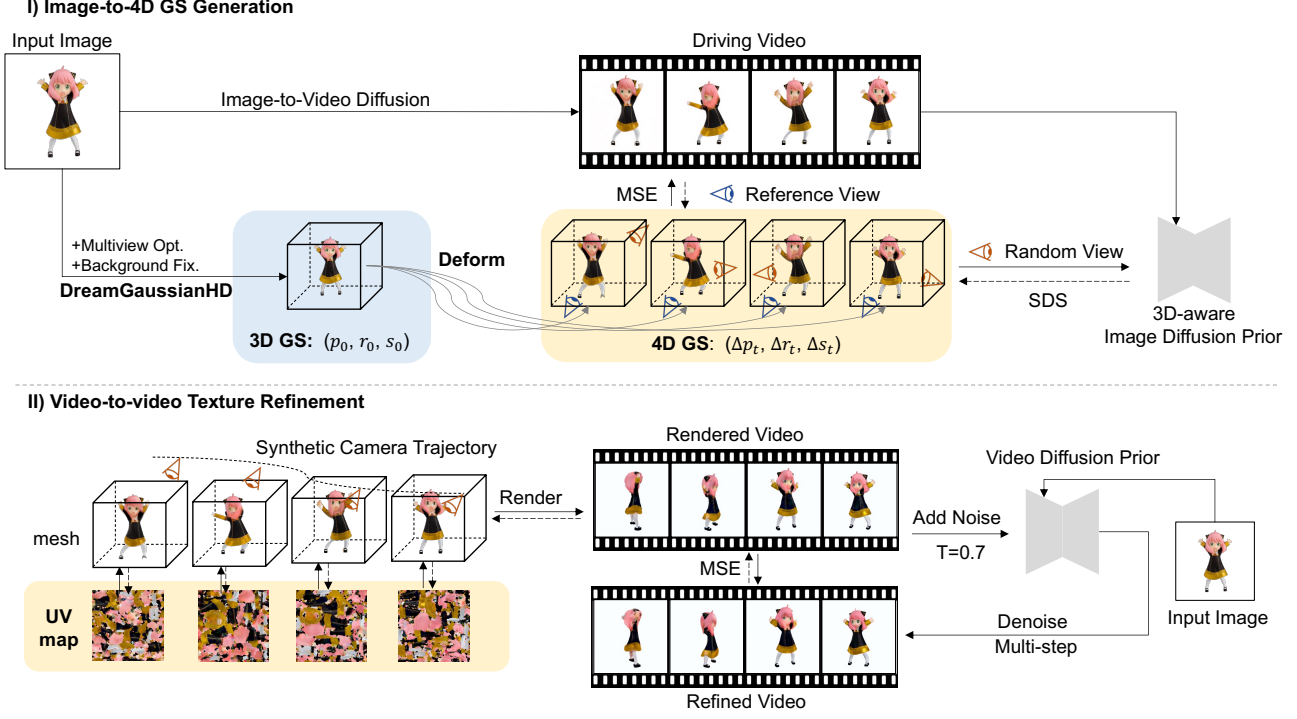


Figure 2: **DreamGaussian4D Framework.** We first obtain a static 3D GS model using DreamGaussianHD and a driving video with an image-to-video diffusion model. We then optimize a deformation network that learns to deform the static 3D GS at different time stamps, supervised by the MSE loss to the driving video and SDS losses. Finally, per-frame meshes can be exported and the texture maps can be refined with a video-to-video pipeline.

### 3.2. Gaussian Deformation for Dynamic Generation

#### 3.2.1. GENERATING DRIVING VIDEO

Different from other methods (Bahmani et al., 2023) that perform SDS supervision using a specific video diffusion model, we propose to use explicit supervision from any video depicting the input image. This video can be created by artists like those in video-to-4D (Jiang et al., 2023), or generated automatically from an image-to-video model. In practice, we use the off-the-shelf Stable Diffusion Video (Blattmann et al., 2023) to generate the videos from input images:

$$\{I_{\text{Ref}}\}_{\tau=1}^T = f_{\psi}(\epsilon; I_{\text{Input}}), \quad (1)$$

where  $I_{\text{Input}}$  represents the input image,  $\{I_{\text{Ref}}\}_{\tau=1}^T$  is the driving video,  $\epsilon$  denotes random noise, and  $f_{\psi}$  is the image-to-video diffusion model. Since our method does not rely on the video diffusion model later, we can choose high-quality videos with better temporal consistency and motion generated by different random seeds, which enables better controllability and diversity for image-to-4D generation.

#### 3.2.2. STATIC-TO-DYNAMIC INITIALIZATION

To further augment the static 3D Gaussians into dynamic 4D Gaussians, a deformation network is trained to predict the change of position, rotation, and scale of each Gaussian given a timestamp.

$$S' = \phi(S, \tau), \quad (2)$$

where  $\phi$  is the deformation network,  $S$  is the spatial descriptions of the static 3D GS including position, rotation, and scaling,  $\tau$  is the time stamp, and  $S'$  is the deformed 3D GS spatial descriptions. However, randomly initializing the deformation network can cause a divergence between the dynamic and static models, leading to convergence at a sub-optimal mode, as exemplified in Figure 8. To mitigate this, we initialize the deformation model to predict zero deformation at the start of training. Concretely, we initialize the weight and bias of the final prediction heads to zero. To enable gradient backpropagation, skip connections are introduced to the prediction heads.

#### 3.2.3. DEFORMATION FIELD OPTIMIZATION

We optimize the deformation field given the driving video from the reference view. We fix the camera to the reference



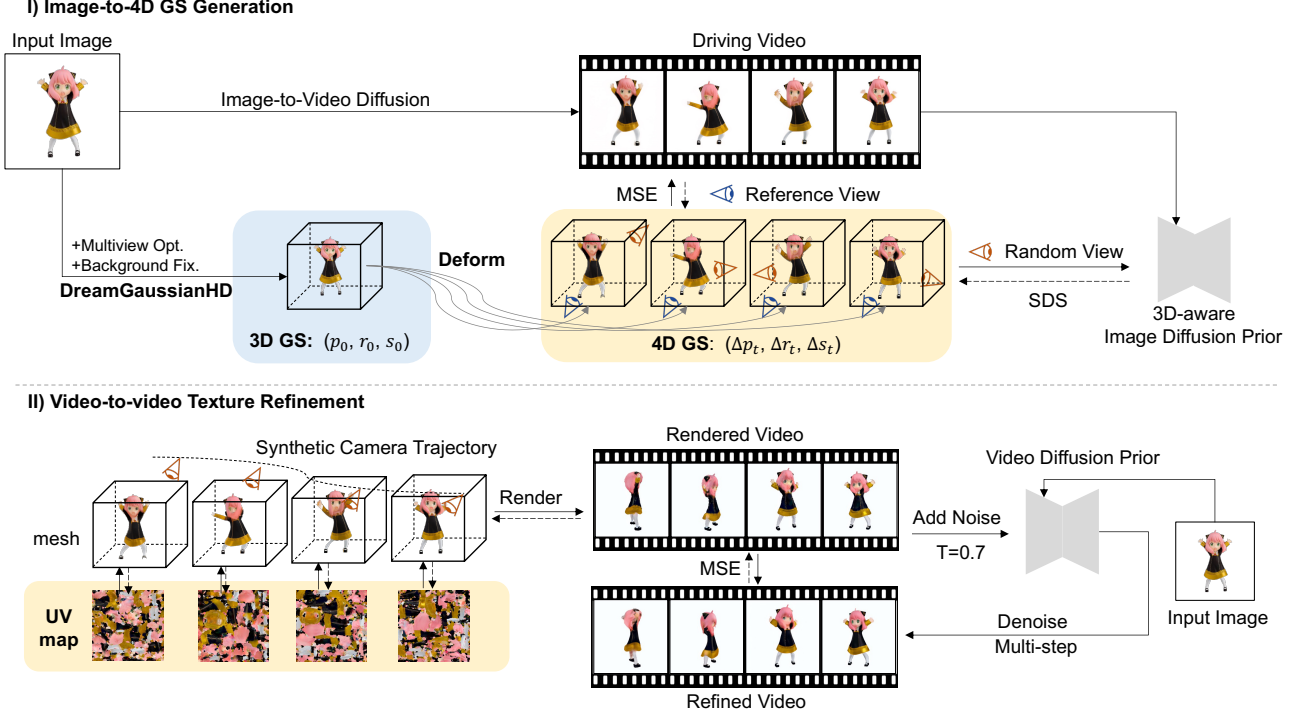


Figure 3: **DreamGaussian4D Framework.** We first obtain a static 3D GS model using DreamGaussianHD and a driving video with an image-to-video diffusion model. We then optimize a deformation network that learns to deform the static 3D GS at different time stamps, supervised by the MSE loss to the driving video and SDS losses. Finally, per-frame meshes can be exported and the texture maps can be refined with a video-to-video pipeline.

view, and minimize the Mean Squared Error (MSE) between the rendered image and the driving video frame at each timestamp:

$$\mathcal{L}_{\text{Ref}} = \frac{1}{T} \sum_{\tau=1}^T \|f(\phi(S, \tau), o_{\text{Ref}}) - I_{\text{Ref}}^{\tau}\|_2^2, \quad (3)$$

where  $I_{\text{Ref}}^{\tau}$  is the  $\tau$ -th frame in the video,  $o_{\text{Ref}}$  is the reference view point and  $f$  is the rendering function. To propagate the motion from the reference view to the whole 3D model, we leverage Zero-1-to-3-XL (Deitke et al., 2023a) to predict the deformation of the unseen part. Although image diffusion models only perform per-frame prediction, the temporal consistency can be mostly preserved since the color and opacity of the static 3D GS are fixed. Similar to the training practice in DreamGaussianHD, multiple views are sampled for each time step.

$$\nabla_{\phi} \mathcal{L}_{\text{SDS}} = \mathbb{E}_{t, \tau, \epsilon, o} [(\epsilon_{\theta}(\hat{I}; t, I_{\text{Ref}}^{\tau}, o) - \epsilon) \frac{\partial I}{\partial \phi}], \quad (4)$$

$$\hat{I} = f(\phi(S, \tau), o), \quad (5)$$

where  $\epsilon$  is a random noise,  $\epsilon_{\theta}$  is the noise predictor of a 3D-aware image diffusion model, and  $o$  is a random viewpoint.

Thanks to the static model initialization, we can start the SDS at a lower noise level. Specifically, we start SDS with a  $T_{\text{max}} = 0.5$ , which is lower than the common practice where  $T_{\text{max}} = 0.98$ .

### 3.3. Video-to-video Texture Refinement

Mesheres for each frame can be extracted similarly to DreamGaussian (Tang et al., 2023a), which involves running local density queries and color back-projection. However, these per-frame meshes lack temporal association, and refining their textures separately can result in flickering as demonstrated in Figure 10. To enhance the UV-space texture map while maintaining temporal consistency, we employ a video-to-video pipeline. This process begins with synthesizing a camera trajectory, where the camera moves at a constant speed along 0 elevations from a randomly chosen horizontal angle. We then render the video and introduce noise at level 0.7 to it. Finally, an image-to-video diffusion model is utilized to transform this noisy video into a clean, denoised version:

$$\{I_{\text{Refined}}\}_{\tau=1}^T = f_{\psi}(\{\hat{I}\}_{\tau=1}^T + \epsilon; I_{\text{Input}}), \quad (6)$$



Figure 4: **Qualitative results.** Renders are shown with gradually changing time stamps and view angles.

where  $\epsilon$  is a random noise at the specified level and  $\{\hat{I}\}_{\tau=1}^{\mathcal{T}}$  is the rendered video. The MSE loss is computed between the two videos:

$$\mathcal{L}_{\text{Refine}} = \|\{\hat{I}\}_{\tau=1}^{\mathcal{T}} - \{I_{\text{Refined}}\}_{\tau=1}^{\mathcal{T}}\|_2^2 \quad (7)$$

The loss is then back-propagated to improve the texture maps at all time steps.

## 4. Experiments

### 4.1. Implementation Details

We run all experiments on a single 80 GB A100 GPU. We implement the DreamGaussian4D framework on the open-source repositories DreamGaussian (Tang et al., 2023a) and 4D Gaussian Splatting (Wu et al., 2023). For driving video generation, we use Stable Video Diffusion to generate 14 frames. For static optimization, we run 500 iterations with

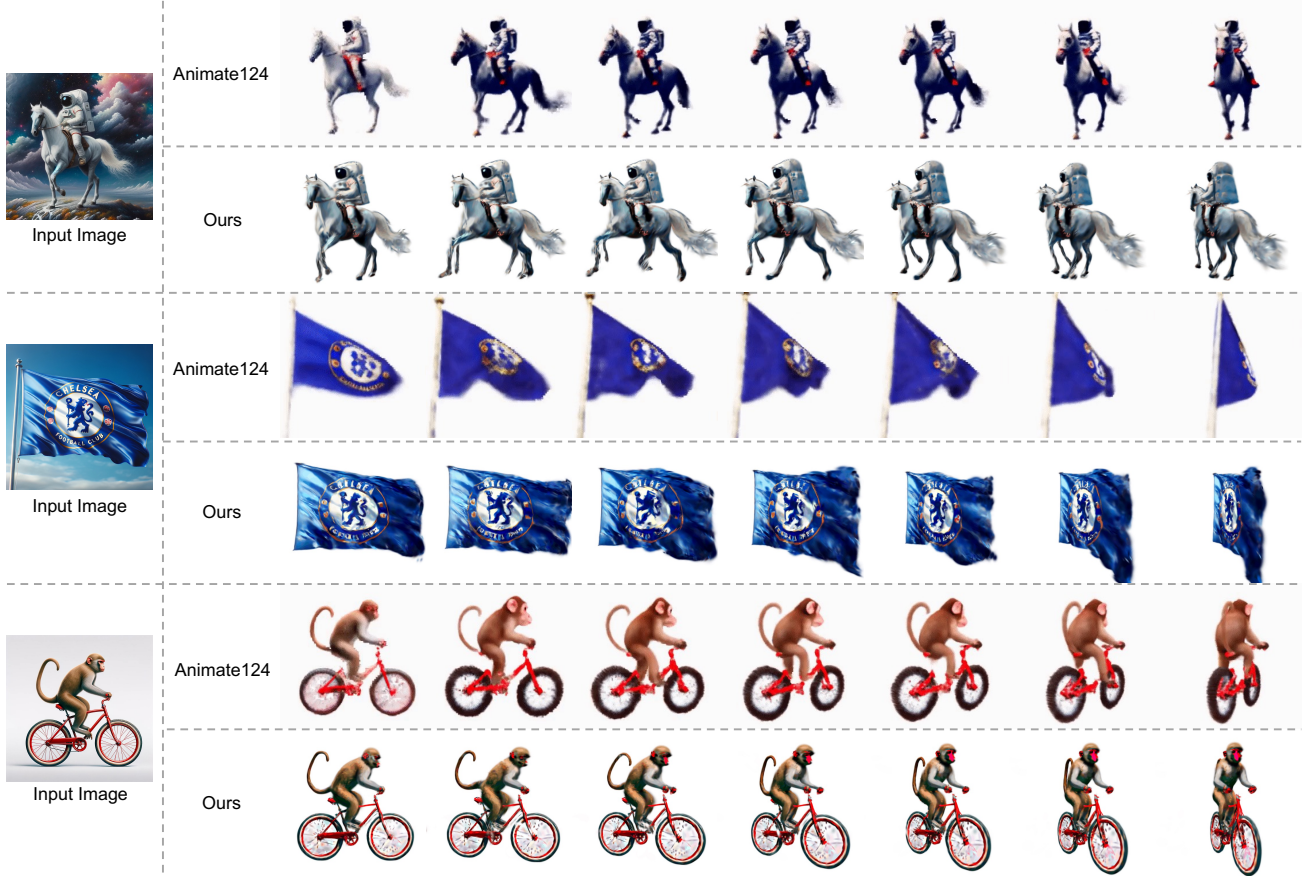


Figure 5: **Comparison with Animate124 (Zhao et al., 2023)**. Our model achieves better faithfulness to the input image, larger motions, and a higher level of detail.

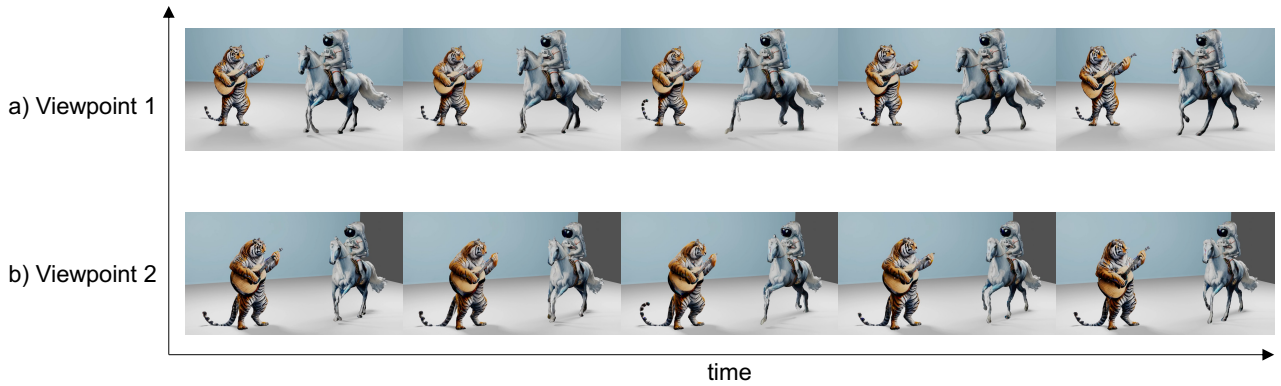


Figure 6: **Composited scene**. 4D GS can be exported to meshes that can be efficiently composited and rendered in Blender.

a batch size of 16 for 2 minutes. We linearly decay  $T_{\max}$  from 0.98 to 0.02. For dynamic representation, we run 200 iterations with batch size 4 for 4.5 minutes, with  $T_{\max}$  linearly decaying from 0.5 to 0.02. For the optional mesh refinement, we run 50 iterations with a constant  $T = 0.7$

for 3.5 minutes.

#### 4.2. Quantitative Results

We evaluate on examples provided in Animate124 (Zhao et al., 2023). For the evaluation metric, we compute CLIP-I.



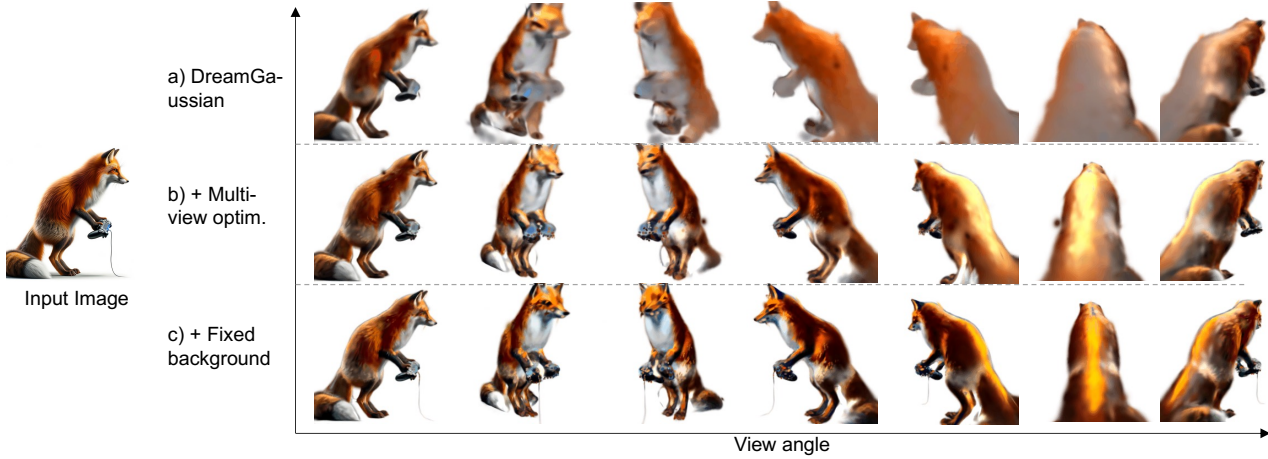


Figure 7: **Ablation on DreamGaussianHD.** Off-the-shelf DreamGaussian suffers from severe blurriness on novel views. Multi-view optimization significantly improves the texture and geometries. Fixing the background color further enhances the level of detail.

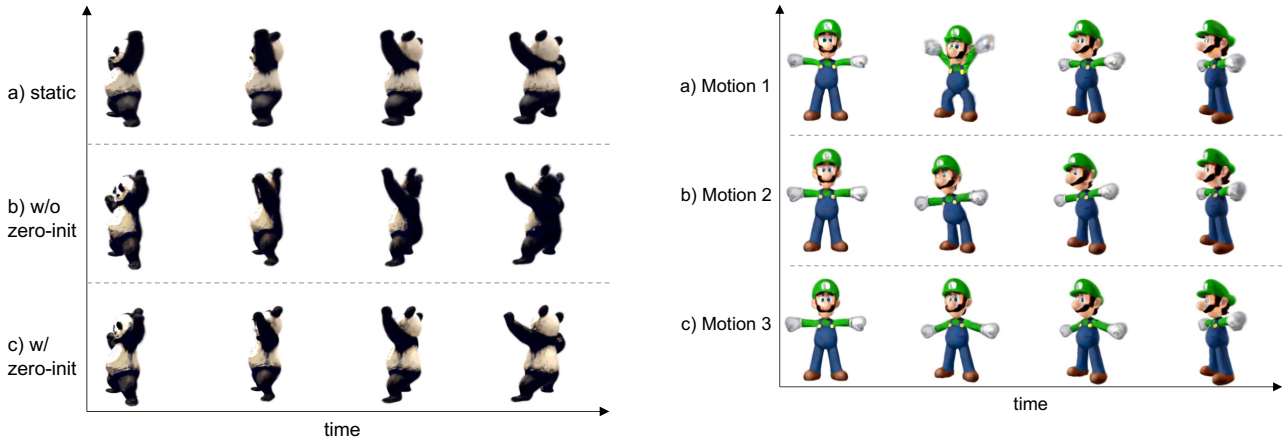


Figure 8: **Ablation on zero-initialization.** Non-zero initialization leads to changes from the static model which leads to sub-optimal modes, *e.g.*, the back of the panda turns fully black. Zero-initialization prevents the drifting.

CLIP-I measures the cosine similarity of CLIP image embedding between reference-view renders and the reference image. The result is provided in Table 2. DreamGaussian achieves the best similarity to the input image. We also compare the running speed in Table 1. DreamGaussian4D reduces the optimization time from hours to minutes.

### 4.3. Qualitative Results

We show qualitative image-to-4D results in Figure 4. The results are rendered in different time steps and camera views. In Figure 5, we compare our approach with Animate124.

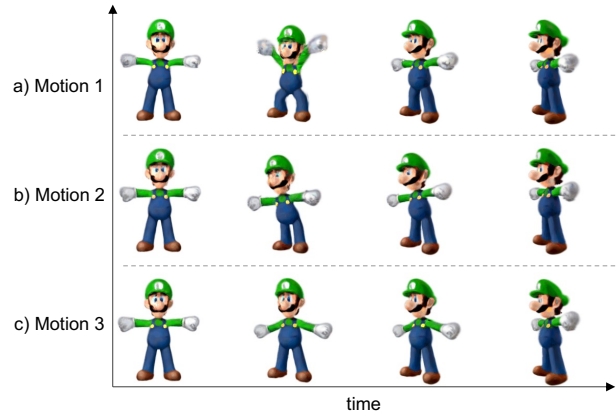


Figure 9: **Controllable Motions.** DreamGaussian4D allows easy control of the generated motions. Different 3D motions can be generated from different driving videos for the same input image.

Our approach achieves better faithfulness to the input image, stronger motion, and richer details in geometry and texture. We further export 4D GS to meshes with texture refinement and composite them in the Blender engine. We render the composited scene from different view angles in Figure 6. All qualitative results are better viewed in videos on the project page.



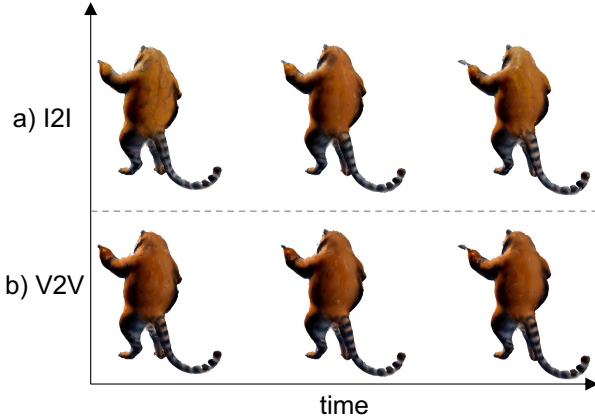


Figure 10: **Ablation on texture refinement.** DreamGaussian-like image-to-image (I2I) optimization leads to poor temporal consistency and flickering in adjacent frames. Video-to-video (V2V) optimization alleviates the issue.

Table 2: **Quantitative Results.** †: computed on 8 examples available at Zhao et al. (2023).

Method	CLIP-I
Zero-1-to-3-V	0.7925
RealFusion-V	0.8026
Animate124 (Zhao et al., 2023)	0.8544
Ours <sup>†</sup>	<b>0.9227</b>

#### 4.4. Ablation

##### 4.4.1. DREAMGAUSSIANHD

We ablate the improvement in image-to-3D quality of DreamGaussianHD in Figure 7. We observe severe blurriness in DreamGaussian, particularly from side views and back views. By introducing multi-view optimization and background fixing, the novel view quality is significantly improved.

##### 4.4.2. ZERO-INITIALIZATION

Without zero-initialization, the dynamic model can be slightly different from the static model at the start of the optimization and the difference could signify in the optimization process, resulting in sub-optimal results. In Figure 8, the back of the panda was black and white in the static stage. However, when initialized differently, the back could turn fully black after dynamic optimization. The issue is resolved by zero-initialization.

##### 4.4.3. DIVERSE MOTIONS

Different from most existing 4D generation approaches (Bahmani et al., 2023; Jiang et al., 2023) using SDS, our method allows better controllability and more diversity in the motions. Different 4D motions can be generated from different driving videos. In Figure 9, we generate three different driving videos for an input image, which results in three different 3D motions.

##### 4.4.4. VIDEO-TO-VIDEO TEXTURE REFINEMENT

Since per-frame meshes have individual texture maps, there is no temporal consistency restriction in the representation. As shown in Figure 10, directly optimizing the texture maps using DreamGaussian-like refinement results in flickering in adjacent frames. Instead, video diffusion models provide temporal consistency and result in smoother temporal changes.

## 5. Conclusion

We propose DreamGaussian4D, a framework that generates 4D contents employing 4D Gaussian Splatting. We show that explicit modeling of spatial transformations in the Gaussian Splatting greatly simplifies the 4D generation task. DreamGaussian4D significantly reduces the optimization time from several hours to several minutes. Moreover, driving motion using generated videos allows explicit control of the 3D motion for the first time. Lastly, DreamGaussian4D allows mesh extraction and temporally-coherent texture optimization, which facilitates real-world applications.

## References

- Abou-Chakra, J., Dayoub, F., and Sünderhauf, N. Particlenerf: A particle-based encoding for online neural radiance fields. In *Proceedings of the IEEE/CVF Winter Conference on Applications of Computer Vision*, pp. 5975–5984, 2024.
- Bahmani, S., Skorokhodov, I., Rong, V., Wetzstein, G., Guibas, L., Wonka, P., Tulyakov, S., Park, J. J., Tagliasacchi, A., and Lindell, D. B. 4d-fy: Text-to-4d generation using hybrid score distillation sampling. *arXiv preprint arXiv:2311.17984*, 2023.
- Blattmann, A., Dockhorn, T., Kulal, S., Mendelevitch, D., Kilian, M., Lorenz, D., Levi, Y., English, Z., Voleti, V., Letts, A., et al. Stable video diffusion: Scaling latent video diffusion models to large datasets. *arXiv preprint arXiv:2311.15127*, 2023.
- Cao, A. and Johnson, J. Hexplane: A fast representation for dynamic scenes. In *Proceedings of the IEEE/CVF Conference on Computer Vision and Pattern Recognition*, pp. 130–141, 2023.
- Chang, A. X., Funkhouser, T., Guibas, L., Hanrahan, P., Huang, Q., Li, Z., Savarese, S., Savva, M., Song, S., Su, H., et al. Shapenet: An information-rich 3d model repository. *arXiv preprint arXiv:1512.03012*, 2015.
- Chen, R., Chen, Y., Jiao, N., and Jia, K. Fantasia3d: Disentangling geometry and appearance for high-quality text-to-3d content creation. *arXiv preprint arXiv:2303.13873*, 2023.
- Chen, Z. and Zhang, H. Learning implicit fields for generative shape modeling. In *Proceedings of the IEEE/CVF Conference on Computer Vision and Pattern Recognition*, pp. 5939–5948, 2019.
- Chen, Z., Tagliasacchi, A., and Zhang, H. Bsp-net: Generating compact meshes via binary space partitioning. In *Proceedings of the IEEE/CVF Conference on Computer Vision and Pattern Recognition*, pp. 45–54, 2020.
- Deitke, M., Liu, R., Wallingford, M., Ngo, H., Michel, O., Kusupati, A., Fan, A., Laforte, C., Voleti, V., Gadre, S. Y., et al. Objaverse-xl: A universe of 10m+ 3d objects. *arXiv preprint arXiv:2307.05663*, 2023a.
- Deitke, M., Schwenk, D., Salvador, J., Weihs, L., Michel, O., VanderBilt, E., Schmidt, L., Ehsani, K., Kembhavi, A., and Farhadi, A. Objaverse: A universe of annotated 3d objects. In *CVPR*, pp. 13142–13153, 2023b.
- Du, Y., Zhang, Y., Yu, H.-X., Tenenbaum, J. B., and Wu, J. Neural radiance flow for 4d view synthesis and video processing. In *2021 IEEE/CVF International Conference on Computer Vision (ICCV)*, pp. 14304–14314. IEEE Computer Society, 2021.
- Duggal, S. and Pathak, D. Topologically-aware deformation fields for single-view 3d reconstruction. In *CVPR*, pp. 1536–1546, 2022.
- Fang, J., Yi, T., Wang, X., Xie, L., Zhang, X., Liu, W., Nießner, M., and Tian, Q. Fast dynamic radiance fields with time-aware neural voxels. In *SIGGRAPH Asia 2022 Conference Papers*, pp. 1–9, 2022.
- Fridovich-Keil, S., Meanti, G., Warburg, F. R., Recht, B., and Kanazawa, A. K-planes: Explicit radiance fields in space, time, and appearance. In *Proceedings of the IEEE/CVF Conference on Computer Vision and Pattern Recognition*, pp. 12479–12488, 2023.
- Gao, C., Saraf, A., Kopf, J., and Huang, J.-B. Dynamic view synthesis from dynamic monocular video. In *Proceedings of the IEEE/CVF International Conference on Computer Vision*, pp. 5712–5721, 2021.
- Guan, S., Deng, H., Wang, Y., and Yang, X. Neurofluid: Fluid dynamics grounding with particle-driven neural radiance fields. In *International Conference on Machine Learning*, pp. 7919–7929. PMLR, 2022.
- Ho, J., Jain, A., and Abbeel, P. Denoising diffusion probabilistic models. *NeurIPS*, 33:6840–6851, 2020.
- Hong, Y., Zhang, K., Gu, J., Bi, S., Zhou, Y., Liu, D., Liu, F., Sunkavalli, K., Bui, T., and Tan, H. Lrm: Large reconstruction model for single image to 3d. *arXiv preprint arXiv:2311.04400*, 2023.
- Jiang, Y., Zhang, L., Gao, J., Hu, W., and Yao, Y. Consistent4d: Consistent 360  $\{^\circ\}$  dynamic object generation from monocular video. *arXiv preprint arXiv:2311.02848*, 2023.

- Jun, H. and Nichol, A. Shap-e: Generating conditional 3d implicit functions. *arXiv preprint arXiv:2305.02463*, 2023.
- Kerbl, B., Kopanas, G., Leimkühler, T., and Drettakis, G. 3d gaussian splatting for real-time radiance field rendering. *ToG*, 42(4):1–14, 2023.
- Li, T., Slavcheva, M., Zollhoefer, M., Green, S., Lassner, C., Kim, C., Schmidt, T., Lovegrove, S., Goesele, M., Newcombe, R., et al. Neural 3d video synthesis from multi-view video. In *Proceedings of the IEEE/CVF Conference on Computer Vision and Pattern Recognition*, pp. 5521–5531, 2022.
- Li, Z., Niklaus, S., Snavely, N., and Wang, O. Neural scene flow fields for space-time view synthesis of dynamic scenes. In *Proceedings of the IEEE/CVF Conference on Computer Vision and Pattern Recognition*, pp. 6498–6508, 2021.
- Li, Z., Wang, Q., Cole, F., Tucker, R., and Snavely, N. Dynibar: Neural dynamic image-based rendering. In *Proceedings of the IEEE/CVF Conference on Computer Vision and Pattern Recognition*, pp. 4273–4284, 2023.
- Ling, H., Kim, S. W., Torralba, A., Fidler, S., and Kreis, K. Align your gaussians: Text-to-4d with dynamic 3d gaussians and composed diffusion models. *arXiv preprint arXiv:2312.13763*, 2023.
- Liu, M., Shi, R., Chen, L., Zhang, Z., Xu, C., Wei, X., Chen, H., Zeng, C., Gu, J., and Su, H. One-2-3-45++: Fast single image to 3d objects with consistent multi-view generation and 3d diffusion. *arXiv preprint arXiv:2311.07885*, 2023a.
- Liu, M., Xu, C., Jin, H., Chen, L., Xu, Z., Su, H., et al. One-2-3-45: Any single image to 3d mesh in 45 seconds without per-shape optimization. *arXiv preprint arXiv:2306.16928*, 2023b.
- Liu, R., Wu, R., Van Hoorick, B., Tokmakov, P., Zakharov, S., and Vondrick, C. Zero-1-to-3: Zero-shot one image to 3d object. *arXiv preprint arXiv:2303.11328*, 2023c.
- Luiten, J., Kopanas, G., Leibe, B., and Ramanan, D. Dynamic 3d gaussians: Tracking by persistent dynamic view synthesis. *arXiv preprint arXiv:2308.09713*, 2023.
- Melas-Kyriazi, L., Laina, I., Rupprecht, C., and Vedaldi, A. Realfusion: 360deg reconstruction of any object from a single image. In *CVPR*, pp. 8446–8455, 2023.
- Mildenhall, B., Srinivasan, P. P., Tancik, M., Barron, J. T., Ramamoorthi, R., and Ng, R. Nerf: Representing scenes as neural radiance fields for view synthesis. In *ECCV*, 2020.
- Nichol, A., Jun, H., Dhariwal, P., Mishkin, P., and Chen, M. Point-e: A system for generating 3d point clouds from complex prompts. *arXiv preprint arXiv:2212.08751*, 2022.
- Park, K., Sinha, U., Barron, J. T., Bouaziz, S., Goldman, D. B., Seitz, S. M., and Martin-Brualla, R. Nerfies: Deformable neural radiance fields. In *Proceedings of the IEEE/CVF International Conference on Computer Vision*, pp. 5865–5874, 2021a.
- Park, K., Sinha, U., Hedman, P., Barron, J. T., Bouaziz, S., Goldman, D. B., Martin-Brualla, R., and Seitz, S. M. Hypernerf: A higher-dimensional representation for topologically varying neural radiance fields. *arXiv preprint arXiv:2106.13228*, 2021b.
- Poole, B., Jain, A., Barron, J. T., and Mildenhall, B. Dreamfusion: Text-to-3d using 2d diffusion. *arXiv preprint arXiv:2209.14988*, 2022.
- Pumarola, A., Corona, E., Pons-Moll, G., and Moreno-Noguer, F. D-nerf: Neural radiance fields for dynamic scenes. In *Proceedings of the IEEE/CVF Conference on Computer Vision and Pattern Recognition*, pp. 10318–10327, 2021.
- Qian, G., Mai, J., Hamdi, A., Ren, J., Siarohin, A., Li, B., Lee, H.-Y., Skorokhodov, I., Wonka, P., Tulyakov, S., et al. Magic123: One image to high-quality 3d object generation using both 2d and 3d diffusion priors. *arXiv preprint arXiv:2306.17843*, 2023.
- Rombach, R., Blattmann, A., Lorenz, D., Esser, P., and Ommer, B. High-resolution image synthesis with latent diffusion models. In *CVPR*, pp. 10684–10695, 2022.

- Shao, R., Zheng, Z., Tu, H., Liu, B., Zhang, H., and Liu, Y. Tensor4d: Efficient neural 4d decomposition for high-fidelity dynamic reconstruction and rendering. In *Proceedings of the IEEE/CVF Conference on Computer Vision and Pattern Recognition*, pp. 16632–16642, 2023.
- Sheynin, S., Ashual, O., Polyak, A., Singer, U., Gafni, O., Nachmani, E., and Taigman, Y. Knn-diffusion: Image generation via large-scale retrieval. *arXiv preprint arXiv:2204.02849*, 2022.
- Shi, R., Chen, H., Zhang, Z., Liu, M., Xu, C., Wei, X., Chen, L., Zeng, C., and Su, H. Zero123++: a single image to consistent multi-view diffusion base model, 2023.
- Singer, U., Sheynin, S., Polyak, A., Ashual, O., Makarov, I., Kokkinos, F., Goyal, N., Vedaldi, A., Parikh, D., Johnson, J., et al. Text-to-4d dynamic scene generation. *arXiv preprint arXiv:2301.11280*, 2023.
- Szymanowicz, S., Rupprecht, C., and Vedaldi, A. Splatter image: Ultra-fast single-view 3d reconstruction. *arXiv preprint arXiv:2312.13150*, 2023.
- Tang, J., Ren, J., Zhou, H., Liu, Z., and Zeng, G. Dreamgaussian: Generative gaussian splatting for efficient 3d content creation. *arXiv preprint arXiv:2309.16653*, 2023a.
- Tang, J., Wang, T., Zhang, B., Zhang, T., Yi, R., Ma, L., and Chen, D. Make-it-3d: High-fidelity 3d creation from a single image with diffusion prior. *arXiv preprint arXiv:2303.14184*, 2023b.
- Tretschk, E., Tewari, A., Golyanik, V., Zollhöfer, M., Lassner, C., and Theobalt, C. Non-rigid neural radiance fields: Reconstruction and novel view synthesis of a dynamic scene from monocular video. In *Proceedings of the IEEE/CVF International Conference on Computer Vision*, pp. 12959–12970, 2021.
- Trevithick, A. and Yang, B. Grf: Learning a general radiance field for 3d representation and rendering. In *ICCV*, pp. 15182–15192, 2021.
- Turki, H., Zhang, J. Y., Ferroni, F., and Ramanan, D. Suds: Scalable urban dynamic scenes. In *Proceedings of the IEEE/CVF Conference on Computer Vision and Pattern Recognition*, pp. 12375–12385, 2023.
- Wang, Y., Chen, X., Ma, X., Zhou, S., Huang, Z., Wang, Y., Yang, C., He, Y., Yu, J., Yang, P., et al. Lavie: High-quality video generation with cascaded latent diffusion models. *arXiv preprint arXiv:2309.15103*, 2023.
- Wu, G., Yi, T., Fang, J., Xie, L., Zhang, X., Wei, W., Liu, W., Tian, Q., and Wang, X. 4d gaussian splatting for real-time dynamic scene rendering. *arXiv preprint arXiv:2310.08528*, 2023.
- Xian, W., Huang, J.-B., Kopf, J., and Kim, C. Space-time neural irradiance fields for free-viewpoint video. In *Proceedings of the IEEE/CVF Conference on Computer Vision and Pattern Recognition*, pp. 9421–9431, 2021.
- Xu, Q., Wang, W., Ceylan, D., Mech, R., and Neumann, U. Disn: Deep implicit surface network for high-quality single-view 3d reconstruction. *Advances in neural information processing systems*, 32, 2019.
- Yang, Z., Gao, X., Zhou, W., Jiao, S., Zhang, Y., and Jin, X. Deformable 3d gaussians for high-fidelity monocular dynamic scene reconstruction. *arXiv preprint arXiv:2309.13101*, 2023.
- Yu, X., Xu, M., Zhang, Y., Liu, H., Ye, C., Wu, Y., Yan, Z., Liang, T., Chen, G., Cui, S., and Han, X. Mvimngnet: A large-scale dataset of multi-view images. In *CVPR*, 2023.
- Yuan, W., Lv, Z., Schmidt, T., and Lovegrove, S. Star: Self-supervised tracking and reconstruction of rigid objects in motion with neural rendering. In *Proceedings of the IEEE/CVF Conference on Computer Vision and Pattern Recognition*, pp. 13144–13152, 2021.
- Zhao, Y., Yan, Z., Xie, E., Hong, L., Li, Z., and Lee, G. H. Animate124: Animating one image to 4d dynamic scene. *arXiv preprint arXiv:2311.14603*, 2023.
- Zheng, Y., Li, X., Nagano, K., Liu, S., Hilliges, O., and De Mello, S. A unified approach for text-and image-guided 4d scene generation. *arXiv preprint arXiv:2311.16854*, 2023.